HHS Public Access

Author manuscript

Nat Chem Biol. Author manuscript; available in PMC 2018 January 10.

Published in final edited form as:

Nat Chem Biol. 2017 September ; 13(9): 961–967. doi:10.1038/nchembio.2433.

Allosteric Sensitization of Pro-Apoptotic BAX

Jonathan R. Pritz[1,†], **Franziska Wachter**[1,†], **Susan Lee**[1], **James Luccarelli**[1], **Thomas E. Wales**[2], **Daniel T. Cohen**[1], **Paul W. Coote**[3], **Gregory J. Heffron**[3], **John R. Engen**[2], **Walter Massefski**[3,4], and **Loren D. Walensky**[1,*]

[1]Department of Pediatric Oncology and the Linde Program in Cancer Chemical Biology, Dana-Farber Cancer Institute, Harvard Medical School, Boston, MA 02215

[2]Department of Chemistry and Chemical Biology, Northeastern University, Boston, Massachusetts, 02115

[3]Department of Biological Chemistry and Molecular Pharmacology, Harvard Medical School, Boston, Massachusetts, 02115

[4]Department of Cancer Biology, Dana-Farber Cancer Institute, Boston, Massachusetts, 02215

Abstract

BAX is a critical apoptotic regulator that can be transformed from a cytosolic monomer into a lethal mitochondrial oligomer, yet drug strategies to modulate it are underdeveloped due to longstanding difficulties in conducting screens on this aggregation-prone protein. Here, we overcame prior challenges and performed an NMR-based fragment screen of full-length human BAX. We identified a compound that sensitizes BAX activation by binding to a pocket formed by the junction of the α3/α4 and α5/α6 hairpins. Biochemical and structural analyses revealed that the molecule sensitizes BAX by allosterically mobilizing the α1–α2 loop and BAX BH3 helix, two motifs implicated in the activation and oligomerization of BAX, respectively. By engaging a region of core hydrophobic interactions that otherwise preserve the BAX inactive state, the identified compound informs fundamental mechanisms for conformational regulation of BAX and provides a new opportunity to reduce the apoptotic threshold for potential therapeutic benefit.

Introduction

BCL-2-associated X protein (BAX) is a 21 kDa globular protein composed of nine α-helices and functions as a critical effector of the BCL-2 family-regulated mitochondrial apoptotic

*Correspondence: Loren D. Walensky, MD, PhD, Dana-Farber Cancer Institute, 450 Brookline Avenue, LC3216, Boston, MA 02215, Loren_Walensky@dfci.harvard.edu, 617-632-6307.

†Authors contributed equally to this work

Author Contributions: J.R.P., F.W., J.L., G.J.H., W.M., S.L., T.E.W., J.R.E., and L.D.W. designed the study; J.R.P., F.W., and D.T.C. generated BAX protein and J.R.P. conducted NMR experiments under the guidance of G.J.H., W.M., J.L., and L.D.W.; G.J.H, P.W.C., and W.M. analyzed screening results utilizing software developed by P.W.C.; J.R.P. and F.W. performed biochemical and mitochondrial assays; J.L. performed the docking calculations and molecular dynamics simulations; S.L. and T.E.W. executed the HXMS experiments under the guidance of J.R.E.; all authors analyzed the data; and J.R.P, F.W., and L.D.W. wrote the manuscript, which was reviewed by all co-authors.

Competing Financial Interests Statement: L.D.W. is a scientific advisory board member and consultant for Aileron Therapeutics.

pathway. An α5/α6 hairpin forms the protein's hydrophobic core, the juxtaposition of α-helices 1 and 6 creates a ligand-interaction surface that regulates the initiation of BAX activation, and at the opposite face of the protein the auto-inhibitory α9 helix resides in a hydrophobic groove composed of portions of α-helices 2, 3 and 4[1]. For such a small protein, a surprisingly large series of regulatory surfaces and complex conformational changes have been defined (Fig. 1a). In its conformationally inactive state, BAX is predominantly cytosolic and may also cycle to and from the mitochondrial outer membrane (MOM) region through a retrotranslocation process mediated by anti-apoptotic proteins, such as BCL-X_L[2]. In response to stress, BH3-only direct activator proteins, such as BIM, BID, and PUMA, can directly engage an α1/α6 binding site, which triggers the initiating conformational changes of BAX activation; this dynamic step may be followed by transient BH3-interactions with the canonical hydrophobic groove to propagate BAX homo-oligomerization[3-6]. In contrast, the canonical groove of anti-apoptotic BCL-2 family members, the BCL-2 BH4 motif, and the cytomegalovirus vMIA protein can bind to and inhibit BAX[7-9]. BAX's central role in apoptosis induction derives from its capacity to undergo a major conformational change that results in irreversible mitochondrial translocation, intramembrane homo-oligomerization, and MOM poration[10]. Indeed, the inherent risk to the cell of renegade BAX activation may underlie the mechanistic basis for its multifaceted regulation.

Given the central role of BCL-2 family proteins in apoptosis regulation during health and disease, a major pharmaceutical effort has been underway for two decades to disarm anti-apoptotic proteins in cancer, where sequestration and inactivation of pro-apoptotic members drives cellular immortality. Specifically, the mechanism by which anti-apoptotic proteins such as BCL-2 deploy a surface groove to trap the apoptosis-triggering BCL-2 homology 3 (BH3) helices of pro-apoptotic proteins, has now been drugged by venetoclax, a selective BCL-2 pocket inhibitor[11,12]. This “inhibit the inhibitor” therapeutic strategy is being applied to develop drugs against the broad spectrum of anti-apoptotic targets implicated in cancer, including BCL-X_L[13-15], MCL-1[16-21], and BFL-1/A1[22].

Having discovered an α1/α6 trigger site for direct BAX activation by pro-apoptotic BH3 domains, we reasoned that an “activate the activators” strategy to drive cancer cell death also warranted therapeutic exploration[5,6]. We previously initiated this effort by *in silico* screening because, in contrast to the highly stable anti-apoptotic targets, the production of BAX for direct, experimental screening was hampered by the challenges in expressing sufficient quantities of recombinant BAX and the general instability of BAX in solution, especially when exposed to potential activators. Previously, our *in silico* and follow-up biochemical and cellular validation efforts yielded the first direct and selective BAX activator molecules (BAMs)[23]. Here, we sought to expand the repertoire of BAX-activating compounds[23-26] for potential clinical development by overcoming prior logistical challenges and directly executing a small molecule fragment screen by nuclear magnetic resonance (NMR) spectroscopy. Intriguingly, we discovered a fragment that engages BAX at a deep hydrophobic pocket in a region that can otherwise be naturally occluded by the BAX-inhibitory BH4 domain of BCL-2[7] or cytomegalovirus vMIA peptide[8]. What's more, molecular interaction at this site sensitizes BAX by inducing allosteric conformational changes of the α1–α2 loop and the BAX BH3 helix, highlighting key mechanistic steps involved in BH3-mediated direct activation and homo-oligomerization of BAX[5,27].

Results

An NMR Screen Identifies Molecular Sensitizers of BAX

To generate recombinant, full-length, monomeric BAX of sufficient quantity and stability to execute a molecular fragment screen, we scaled up our production method to an overall culture volume of 48 liters, and then performed sequential lysis of bacterial pellets at 4°C using a microfluidizer, followed by batch binding of the lysate to chitin affinity resin, dithiothreitol (DTT) elution, and purification by size exclusion chromatography (Supplementary Results, Supplementary Fig. 1a–b). Using this approach, we were able to generate 22 mg of BAX protein at a concentration of 0.6 mg/mL for initial screening, representing an overall yield of 0.5 mg of pure, full-length protein per liter of bacterial culture. We further confirmed by HSQC NMR analysis that our preparation of recombinant, full-length BAX monomer was stable for days at room temperature, enabling us to embark on a small molecule screening effort (Supplementary Fig. 1c).

We employed fragment screening by saturation transfer difference (STD) NMR to identify molecules that interact with BAX. This approach couples the efficiency of small molecular fragments (<300 Da) in sampling chemical interaction space[28] with the sensitivity to detect relatively weak ligand binding[29]. STD NMR measures the change in ^{1}H-NMR signal of a ligand following selective irradiation of the target protein, where transfer of magnetization from protein to ligand causes a decrease in signal that reflects ligand-protein interaction. The rapid acquisition time, relative ease of analysis, and the ability to pool compounds with non-overlapping ^{1}H-NMR spectra made STD NMR a tractable platform for advancing a fragment-based screen of pro-apoptotic BAX[30].

The Maybridge Ro3 library of 1000 molecular fragments was first subjected to a quality control workflow to eliminate any fragments that exhibited poor solubility, aggregation below 500 μM, or whose NMR spectra were not consistent with the chemical structure. The 960 compounds that passed this quality control step were characterized by ^{1}H-NMR and pooled in groups of ten such that spectral overlap was minimized. Of the 96 pools analyzed, we detected a positive STD signal in 37, which represented 86 individual hits that were then rescreened in pools of three, ultimately yielding 56 confirmed interactors (Supplementary Table 1, Fig. 1b). Fifty-three commercially available fragments were ordered, retested by STD as singletons, and confirmed as BAX-Interacting Fragments (BIFs) (Supplementary Table 2). Nearly half of the identified BIFs were composed of linked or fused five and six-membered rings (Supplementary Table 3). To determine if any of the identified BIFs influenced the function of BAX, we screened the 53 BIFs in a liposomal release assay designed to identify both (1) direct BAX activators and (2) sensitizers or inhibitors of direct BAX activation induced by a stapled BIM BH3 helix, BIM SAHB$_{A2}$ (aa 145–164)[6]. First, baseline fluorescence with liposomes and compound alone was read, followed by the addition of BAX to evaluate for direct activation; then, BIM SAHB$_{A2}$ was added to this mixture and the effect of the combination monitored, and compared with the triggering activity of BIM SAHB$_{A2}$ and BAX in the absence of compound. Using this assay format, we identified 4 direct activators of BAX-mediated liposomal release and 8 sensitizers of BIM SAHB$_{A2}$-triggered, BAX activation (Supplementary Table 1). The direct activator profile is

exemplified by the positive control BIM SAHB$_{A2}$ peptide, which induces time-responsive liposomal release in the presence of BAX (Fig. 1c, Supplementary Table 4). A novel sensitizer profile was most strikingly reflected by the activity of BIF-44 (**1**), which had a minimal effect on BAX when incubated as a single agent, but when combined with BIM SAHB$_{A2}$ enhanced both the kinetics and maximal amount of BAX-mediated release as compared to treatment with BIM SAHB$_{A2}$ alone (Fig. 1c).

Given these intriguing results, we subjected BIF-44 to a rigorous workflow of validation studies. First, we sought to corroborate our BIF-44/BAX interaction findings based on STD with an orthogonal NMR measure (Fig. 2a). We applied Carr–Purcell–Meiboom–Gill (CPMG)-NMR, a method that takes advantage of the faster T2 relaxation time of protein compared to ligand, to monitor for a potential change in BIF-44 signal upon incubation with BAX[30]. The formation of a protein-ligand complex reduces the relaxation time of the ligand, resulting in a measurable decrease in ^{1}H-NMR signal. In the presence of BAX, we indeed observed a sharp reduction in signal, indicative of BIF-44 binding (Fig. 2a). We then quantified the BIF-44/BAX interaction by isothermal calorimetry (ITC), which revealed a K_d of 37 ± 12 μM (Fig. 2b). This double-digit micromolar affinity is both consistent with expectations for a small molecule fragment and the capacity of low affinity interactions to activate BAX. Indeed, in contrast to the nanomolar and subnanomolar affinities required for BH3-only protein and BH3-mimetic inhibition of anti-apoptotic targets, BAX activation occurs by a transient “hit-and-run” mechanism in which ligand-induced α1–α2 loop mobilization and BAX BH3 domain exposure catalyzes signal propagation through subsequent BAX autoactivation[5,31,32].

We further confirmed the sensitization activity of BIF-44 by demonstrating little to no independent triggering effect on BAX-mediated liposomal release when applied using a broad 10–175:1 molar ratio of BIF-44 to BAX (Fig. 2c), but in the presence of BIM SAHB$_{A2}$, BIF-44 dose-responsively enhanced both the kinetics and maximum level of BAX-mediated liposomal release (Fig. 2d, Supplementary Table 4). We also found that the maximum level of liposomal release achieved upon BIF-44 sensitization was independent of the order of addition of the BIF-44 and BIM SAHB$_{A2}$ ligands (Supplementary Fig. 2a–e), and that BIF-44 sensitization extended to other BAX-activation stimuli, including heat[33] and BIM$_L$ protein[34] (Supplementary Fig. 2f–g).

Finally, before advancing the BIF-44/BAX interaction to structural and mechanistic analyses, we sought to rule out non-specific activity that could derive from aggregation of the small molecule fragment. In addition to passing our initial quality control check performed on the Maybridge Ro3 library, we evaluated BIF-44 in a series of aggregation assays alongside positive control aggregator compounds[35]. First, we queried an aggregator web tool (http://advisor.bkslab.org/)[36], which found no structural similarities between BIF-44 and other aggregator compounds in the database. In contrast to the small molecule aggregators 4-aminodiphenylamine (4-ADPA)[36] and tetraiodophenolphthalein (I4PTH)[35], BIF-44 showed no NMR line broadening at the highest micromolar dosing (300 μM) used in our studies (Supplementary Fig. 3a–b). Whereas 4-ADPA demonstrated rapid NMR signal decay over time at 300 μM dosing, the BIF-44 signal was stable at this dose (Supplementary Fig. 3c), and showed little to no difference in decay between 25 and 300 μM dosing when

evaluated at even longer time points (Supplementary Fig. 3d). We then compared BIF-44, 4-ADPA, and I4PTH in dynamic light scattering experiments across a broad micromolar dose range. Whereas 4-ADPA and I4PTH begin to show evidence of light scattering at 300 μM and 10 μM, respectively, BIF-44 showed no such effect even at 1 μM concentration (Supplementary Fig. 3e). Finally, small molecule formation of structured aggregates has also been shown to cause spurious effects on protein targets[35,37]. To rule out this possibility, we compared the morphology of micromolar solutions of I4PTH, a robust aggregator compound, to that of BIF-44 by negative stain electron microscopy. Whereas I4PTH produced prominent, structured aggregates, as previously reported[35], BIF-44 showed no such effect (Supplementary Fig. 3f). In addition, neither small molecule aggregator, 4-ADPA or I4PTH, had any effect on BIM SAHB$_{A2}$-triggered, BAX-mediated liposomal release (Supplementary Fig. 3g–h). Thus, we find by a series of orthogonal measures that BIF-44 demonstrates no evidence of small molecule aggregation even at very high micromolar concentrations and induces a specific sensitizing effect on BAX activation and poration.

To evaluate the structure-based reproducibility and selectivity of the observed BIF-44 activity, we evaluated the binding and functional properties of a series of BIF-44 analogs. Importantly, we find that BIF-44-like diaryl ethers that either shift the hydroxyl from the *para* to the *meta* position (ANA-BIF-1 [**2**]), replace the ether linkage with a methylene group (ANA-BIF-2 [**3**]), or replace the hydroxyl group with an amine in the same position (ANA-BIF-3 [**4**]), all retain BAX-binding activity as assessed by STD NMR, and demonstrate BAX-sensitization activity (Supplementary Fig. 4a–c). In contrast, diaryl ethers that bear a *para*-hydroxyl group in each aromatic ring (ANA-BIF-4 [**5**]), or that replace the BIF-44 hydroxyl with a carboxyl group (ANA-BIF-5 [**6**]), manifest little to no BAX-binding or sensitization activity (Supplementary Fig. 4d–e). These data provide evidence for a structure-activity relationship that supports the specificity of action of BIF-44 in binding to BAX and sensitizing BH3-mediated BAX activation.

Identification of the BIF-44 Binding Site on BAX

In our prior work characterizing direct BAX activator molecules (BAMs), we observed direct competition between BAMs and BIM SAHB$_{A2}$ at the BH3-trigger site[23]. Here, in evaluating the newly-identified BAX-sensitization activity, we surprisingly found that BIM SAHB$_{A2}$ had no effect on the STD signal (Fig. 3a). We confirmed the absence of BIM SAHB$_{A2}$ competition for BIF-44 engagement of BAX using the alternative method of competitive fluorescence polarization assay. For this experiment, we employed the direct interaction between fluorescein isothiocyanate (FITC)-BIM SAHB$_{A2}$ and BAX (Supplementary Fig. 5a) as the basis for comparative competition by N-terminal acetylated BIM SAHB$_{A2}$ and BIF-44. Whereas Ac-BIM SAHB$_{A2}$ dose-responsively competed with FITC-BIM SAHB$_{A2}$ for BAX binding, BIF-44 had little to no effect (Fig. 3b). These data raised the intriguing possibility of an alternative mechanism for BIF-44-mediated sensitization of BAX.

As part of our workflow to screen for compounds that might bind to and inhibit BAX, we also tested whether the identified BIFs could compete with the inhibitory vMIA peptide for BAX interaction. vMIA is a cytomegalovirus protein implicated in blocking BAX-mediated

apoptosis, which ensures host cell survival during viral infection and replication[38,39]. The BAX-binding domain of vMIA achieves its inhibitory effect by binding to a discrete pocket formed by the flexible loops between helices α1/α2, α3/α4, and α5/α6 and a portion of the C-terminal α9 helix, preventing BAX-activating conformational changes by stabilizing the α3/α4 and α5/α6 hairpins[8]. Much to our surprise, we observed both a reduction in the BIF-44 STD signal upon co-incubation with vMIA peptide (Fig. 3c) and dose-responsive displacement of the FITC-vMIA/BAX interaction by BIF-44, as assessed by competitive FPA (Fig. 3d, Supplementary Fig. 5b). A BCL-2 BH4 domain helix, which suppresses BAX activation by engaging a groove formed by α1, α1–α2 loop, and α2/α3 and α5/α6 hairpins in the immediate vicinity of the vMIA binding site[7] (Fig. 1a), also competes with BIF-44 for BAX interaction, as assessed by STD NMR (Supplementary Fig. 6).

Our BIF-44 results presented an intriguing paradox: how could a molecular fragment that sensitizes BH3-triggered BAX activation do so by presumably engaging BAX in a region that mediates BAX inhibition? To address this mechanistic question, we first sought to more definitively determine the BIF-44 binding site on BAX. We performed ^{15}N-BAX NMR upon BIF-44 titration, and identified a series of focal, dose-responsive chemical shift changes that colocalized to the region implicated in the vMIA binding site on BAX (Fig. 3e, Supplementary Fig. 7). The most prominent changes (2 SD) localized to the junction of the α3/α4 and α5/α6 hairpins, which juxtapose to form a binding interface (Fig. 3f). Especially intriguing are more subtle changes (1 SD) that become amplified with increasing BIF-44 dosage and localize both to the internal helical regions of α5 and α6 (BAX's hydrophobic core), and the neighboring internal interaction surfaces between α1 and α2 (Fig. 3e–f and Supplementary Fig. 7), the latter helix being the critical BH3 motif that must become exposed for BAX activation and oligomerization to ensue. Thus, these NMR data not only corroborated our STD and FPA data with respect to BIF-44 competition with vMIA at a strikingly similar interaction site, but also suggested that BIF-44 interaction induces structural changes transmitted through the α5–α6 hydrophobic core to the internal surfaces of α1 and α2, a region implicated in BIM BH3-mediated direct activation of BAX at its N-terminal surface[5,6].

To further develop a mechanistic hypothesis for the sensitization activity of BIF-44, we applied the HSQC NMR results to calculate docked structures of the BIF-44/BAX complex using an ensemble docking protocol incorporating all 20 NMR solution structures[1] (PDB ID 1F16). Eighteen of twenty dockings position BIF-44 at a deep pocket formed by the core hydrophobic α5 and α6 helices and the loop between α3 and α4 (Supplementary Fig. 8a–c). Intriguingly, this pocket emerges as a ligand-binding “hot spot” based on analyses of the BAX structure (PDB ID 1F16) using the FTsite and FTdyn algorithms[40] (Supplementary Fig. 8d–e). We then performed molecular dynamics (MD) simulations that assessed protein movements in the presence or absence of BIF-44 at the docked site. Interestingly, the calculations suggested a specific increase in conformational flexibility involving the α1–α2 region of BAX (Supplementary Fig. 9a–b, Supplementary Videos 1–2), a site that is distant from the BIF-44 docking location but subject to allosteric sensing, as also suggested by the dose-responsive HSQC NMR results (Supplementary Fig. 7). The predicted allosteric increase in α1–α2 loop flexibility was further supported by principal component analysis (PCA) of the MD trajectory, which revealed that BIF-44 binding increased the contribution

of the principle component that corresponded to motion of the α1–α2 loop (Supplementary Fig. 9c–d). Normal mode analysis (NMA) calculations were also performed to evaluate and compare the large-scale motions of the BAX protein in the presence and absence of BIF-44 interaction. Consistent with the difference in root mean square fluctuation (ΔRMSF) and PCA results (Supplementary Fig. 9a–d), the NMA also indicates greater flexibility of the α1–α2 region for the BIF-44/BAX complex compared to BAX alone (Supplementary Fig. 9e–f). The results of these calculations led us to hypothesize that BIF-44 engagement in the vMIA binding region could sensitize BH3-mediated BAX activation through allosteric mobilization of the distinct α1–α2 region, which has been implicated in the initiation of BAX activation[5].

BAX Sensitization by an Allosteric Mechanism

To evaluate whether the BIF-44 sensitization mechanism indeed derives from allosteric mobilization of the α1–α2 region, which is implicated in BH3-mediated initiation of BAX activation via an N-terminal trigger site, we performed comparative hydrogen-deuterium exchange mass spectrometry (HXMS) on a mixture of BAX and liposomes in the presence or absence of BIF-44. Here, we use our liposomal system to explicitly correlate functional activation of BAX, as measured by BAX-mediated liposomal release assay, with conformational modulation in a membrane environment that simulates the physiologic context for regulated BAX activation and poration. HXMS probes protein structure by measuring the deuterium incorporation of backbone amide hydrogens[41]. When diluted into deuterium buffer, backbone hydrogens of flexible and/or exposed protein regions rapidly exchange with deuterium, whereas buried domains and/or those regions that contain hydrogen-bonding involving backbone amide hydrogens (such as in α-helices) demonstrate slowed or suppressed deuterium exchange[42-44]. First, we demonstrate that the deuterium exchange profile of our recombinant, full-length, monomeric BAX preparation is consistent with the NMR structure (PDB ID 1F16), such that exposed regions are progressively labeled and buried regions are shielded from exchange, and remains similarly stable over time (10 sec, 1 min, 100 min) in the presence or absence of liposomes (Supplementary Fig. 10). Upon incubating BAX with BIF-44 in the liposomal context that supports functional activation of BAX, we reproducibly observe focal deprotection of peptide fragments corresponding to amino acids 46–62, the very region that encompasses the distal portion of the α1–α2 loop and proximal half of the α2 BH3 helix (Fig. 4a–b, Supplementary Fig. 11a). To further validate the specificity of this finding, we tested the influence of two antibodies, which bind to discrete regions of BAX, on the observed BIF-44-induced deprotection. We reasoned that if BIF-44 was specifically mobilizing or exposing the BH3 region of BAX, a BAX-BH3-specific antibody would promptly bind and suppress access of this region to deuterium exchange. Conversely, an antibody such as 6A7 that binds to an alternate region of the protein, which becomes exposed upon BH3-triggered BAX activation (aa 12–24)[6,45], would serve as a negative control. Indeed, we found that the BH3 antibody selectively suppressed the observed deuterium exchange promoted by BIF-44 in the BAX BH3 region (Fig. 4c), whereas the 6A7 antibody had no inhibitory effect on BIF-44 mediated-deprotection (Fig. 4d). Taken together, the NMR, computational, and HXMS results, are consistent in linking BIF-44 binding at a noncanonical interaction site to allosteric mobilization of the α1–α2 region, where BH3-induced conformational changes initiate BAX activation.

To examine how BIF-44 and BIM SAHB$_{A2}$ engagement at distinct sites synergize to trigger BAX activation, we performed HXMS analyses of BAX in the presence of BIF-44, BIM SAHB$_{A2}$, or the combination. The hydrogen-deuterium exchange profiles of BIM SAHB$_{A2}$ and BIF-44 are notably distinct, consistent with their different sites of engagement and distinct mechanisms of action. Whereas BIM SAHB$_{A2}$ directly binds to the N-terminal trigger site formed by surface residues of α-helices 1 and 6 and displaces the α1–α2 loop leading to 6A7 epitope exposure[5,7], BIF-44 engages a distant site, causing focal allosteric changes localized to the distal α1–α2 loop and proximal α2 BH3 helix (Fig. 5a). Combined treatment amplifies deprotection of the α1–loop–α2 region (Fig. 5a–b) with a deuterium exchange profile that is stable over time (Supplementary Fig. 11b–c), consistent with the ability of BIF-44 to effectively sensitize BIM SAHB$_{A2}$-mediated conformational activation of BAX. Finally, to link these intriguing mechanistic findings to a physiologic context, we tested the capacity of BIF-44 to sensitize BAX-mediated mitochondrial apoptosis, as measured by cytochrome *c* release from treated mouse liver mitochondria. Consistent with the synergy in conformational activation of the BAX N-terminal region, as observed by HXMS, BIF-44 dose-responsively sensitized BIM SAHB$_{A2}$-induced triggering of BAX-mediated cytochrome *c* release from mitochondria (Fig. 5c). Thus, our NMR screen identified a small molecule BAX sensitizer that facilitates the initiation of BH3-mediated direct BAX activation by a novel allosteric mechanism.

Discussion

Allostery has emerged as a key feature of BCL-2 family protein regulation, influencing both the apoptotic response and opportunities to pharmacologically manipulate it. For example, BH3-only triggering of BAX at the α1/α6 interaction site on the N-terminal face of the protein drives release of α9 at the C-terminal face for mitochondrial translocation[5,46], BCL-2 BH4 and vMIA engagement restrict the conformational activation of BAX[7,8], PUMA induces partial unfolding of BCL-X$_L$ to release sequestered p53 from a distal site[47], and covalent modification or mutagenesis of an α6 cysteine of MCL-1 influences the functional activity of its canonical anti-apoptotic binding pocket at the opposite face of the protein[48]. Indeed, one of the cardinal features and mechanistic requirements for activation and homo-oligomerization of the essential executioner proteins of mitochondrial apoptosis, BAX and BAK, involves exposure of their respective BH3 domains, which can either be trapped by the canonical pockets of anti-apoptotic members[12] or remain free to mediate formation of toxic mitochondrial pores[27]. Thus, pharmacologic approaches that induce the release or sequestration of the BAX and BAK BH3 domains stand to directly influence cell fate in a host of diseases.

Here, we report what is, to our knowledge, the first NMR-based small molecule screen of full-length BAX in solution, overcoming prior challenges of generating protein in sufficient quantity and with the required stability to accomplish this goal. Whereas such efforts reported over a decade ago for an anti-apoptotic BCL-2 family member have now led to the first, selective small molecule inhibitor of BCL-2[11,49], an analogous approach applied to BAX has remained out of reach. Using an STD NMR screening strategy, we identified a molecular fragment, BIF-44, with a unique BAX sensitization activity that manifested upon co-incubation of the compound with BAX and a triggering BH3 ligand in a membrane

environment. Paradoxically, the binding site for this molecule was not at one of the established BH3 interaction sites[6,50], but instead at a discrete region previously reported to mediate BAX inhibition by the cytomegalovirus vMIA protein[8]. NMR analysis suggested that molecular interaction transmitted chemical shift changes through the protein core to the N-terminal region of the protein that includes the BH3 helix. MD simulations pointed to enhanced conformational flexibility of the α1–α2 region upon BIF-44 binding, an observation that was further supported by PCA and NMA analyses. Indeed, HXMS studies confirmed that BIF-44 induces deprotection of portions of the α1–α2 loop and BAX BH3 helix, and this focal increase in deuterium exchange was selectively blocked by a BH3, but not 6A7, antibody.

Our results suggest that the identified small molecule binding site, formed by the intersection of the α3/α4 and α5/α6 hairpins, represents a hot spot for allosteric activation of BAX. Targeting and perturbing the α5–α6 hydrophobic core of the BAX protein in this manner provides both an opportunity to develop novel sensitizers of BAX-mediated apoptosis and a physiologic rationale for direct blockade of this region by BAX-inhibitory motifs such as vMIA and BCL-2 BH4. In addition, the allosteric consequences of BIF-44 sensitization, namely synergistic mobilization of the α1–α2 loop and BH3 domain, underscores the mechanistic importance of the N-terminal conformational change to BH3 initiation of BAX activation.

Online Methods

Small molecules—The Ro3 diversity fragment library used for screening by STD NMR was purchased from Maybridge. All BIFs were repurchased for biochemical characterization from Maybridge, with documented purities of ≥95%. BIF-44 (**1**, 4-phenoxyphenol) was also ordered from Alfa Aesar (99% purity). ANA-BIF-1 (**2**, 3-phenoxyphenol) was purchased from Alfa Aesar (98% purity), ANA-BIF-2 (**3**, 4-benzylphenol), ANA-BIF-3 (**4**, 4-phenoxyaniline), and ANA-BIF-5 (**6**, 4-phenoxybenzoic acid) from Sigma-Aldrich (purities of 99%, 97%, and 97%, respectively), and ANA-BIF-4 (**5**, 4,4′-oxydiphenol) from MP Biomedicals (≥95% purity). 4-ADPA (4-aminodiphenylamine) and I4PTH (3′,3″,5′,5″-tetraiodophenolphthalein) were purchased from TCI (>98% and >95% purity, respectively).

Peptide synthesis—Solid-state peptide synthesis using Fmoc chemistry was performed as previously described[51]. The vMIA (^{131}EALKKALRRHRFLWQRRQRA^{150}-$CONH_2$)[8], BCL-2 BH4 $SAHB_A$ (^{13}EIVBKYIHYKLSXRGYXWDA^{32}-$CONH_2$)[7], and BIM $SAHB_{A2}$ (^{145}EIWIAQELRXIGDXFNAYYA^{164}-$CONH_2$)[6] peptides (X, stapling amino acid; B, norleucine) were N-terminally derivatized with either an acetyl group or fluorescein isothiocyanate (FITC)-β-alanine for the indicated applications in NMR and biochemical experiments. Peptides were purified by LC-MS to >95% purity (Supplementary Fig. 12) and quantified by amino acid analysis. Lyophilized peptides were reconstituted in 100% DMSO or DMSO-d_6 and diluted into the indicated aqueous buffers for experimental use.

Expression and purification of full-length BAX—Recombinant, full-length BAX was expressed in BL21 (DE3) *E. coli* using the pTYB1 vector[1,6]. Cell pellets were resuspended in 20 mM Tris, 250 mM NaCl, pH 7.2 and lysed by two passes through a microfluidizer

(Microfluidics) chilled to 4°C. The lysate was clarified by centrifugation at 20,000 rpm. BAX was purified by batch affinity binding at 4°C using chitin resin (New England Biolabs), followed by loading onto gravity flow columns for washing and elution. The intein-chitin binding domain tag was cleaved by 36 hour incubation in 50 mM dithiothreitol at 4°C. Pure protein was isolated by size exclusion chromatography (Superdex 75 10/300; 20 mM HEPES, 150 mM KCl, pH 7.2 or 20 mM potassium phosphate, pH 6.2) using an FPLC system (GE Healthcare Life Sciences).

Fragment screening by STD NMR—Molecular fragments (Ro3 diversity library, Maybridge) were characterized by ^{1}H-NMR and then pooled in groups of 10 to minimize spectral overlap using in-house software. During the process of library curation, ^{1}H-NMR spectra were collected at a concentration of 500 μM in phosphate buffered saline (pH 7.4) and fragments exhibiting poor solubility, aggregation, or whose NMR spectra were inconsistent with the chemical structure (total of 40), were removed prior to pooling. Fragment pools were added to a 5 μM solution of unlabeled, full-length human BAX in 20 mM potassium phosphate buffer, pH 6.2 in 10% (v/v) D_2O, resulting in a final compound concentration of 300 μM. The mixing and loading of samples into a 5-mm NMR tube was performed using a liquid handling robot (Gilson). STD NMR measurements were acquired at 25°C on a Varian Inova 500-MHz spectrometer equipped with a helium-cooled cryoprobe. Low power saturation of the protein was achieved with a series of 50 ms Gaussian pulses for a total of 3 seconds; on-resonance irradiation was performed at 0.8 ppm, and off-resonance irradiation at 30 ppm. Standard excitation sculpting was used for solvent suppression. Each experiment was run for 14 min. The results were initially analyzed by comparing the on and off resonance STD spectra for each pool to determine the presence of binders. Subsequently, each pool was analyzed to identify individual binders using in-house analysis and display software, which allowed for precise alignment of on- and off-resonance spectra. Fragments in pools that yielded a positive STD signal were then subdivided into groups of three for retesting. Those fragments that exhibited STD in both experiments were reordered from Maybridge and tested both as single compounds and in competitive binding experiments.

Liposomal release assay—Large unilamellar vesicles (LUVs) with a lipid composition similar to the outer mitochondrial membrane were formed by liposome extrusion as previously described[52]. Briefly, a lipid mixture containing a 48:28:10:10:4 molar ratio of phosphatidylcholine, phosphatidylethanolamine, phosphatidylinositol, dioleoyl phosphatidylserine, and tetraoleolyl cardiolipin (Avanti Polar Lipids) was generated in chloroform. Lipid films were formed by evaporation of solvent, initially under nitrogen gas and then by overnight vacuum, followed by storage at –80 °C under nitrogen. Lipid films were hydrated in 1 mL assay buffer (10 mM HEPES, 200 mM KCl, 1 mM $MgCl_2$, pH 7.0) and mixed with the fluorophore and quencher pair, 8-aminonaphthalene-1,3,6-trisulfonic acid (ANTS, 12.5 mM) and p-xylene-bis-pyridinium bromide (DPX, 45 mM). Liposomes were formed by 5 freeze/thaw cycles followed by extrusion through a 100 nm polycarbonate membrane and purified using a Sepharose CL-2B size-exclusion column. For measurement of BAX activation, BAX (750 nM) was added to the indicated concentration of molecular fragment in the presence of liposomes, followed by the specified BAX-triggering condition (BIM $SAHB_{A2}$[6], heat[33], or recombinant BIM_L[34]) at the indicated time points. The assay was

carried out in black opaque 384 well plates (30 μl per well). ANTS/DPX release was monitored over time at room temperature in a spectrofluorometer (Tecan Infinite M1000) using an excitation wavelength of 355 nm, an emission wavelength of 540 nm, and a bandwidth of 20 nm. Maximal release was determined by the addition of Triton X-100 to a final concentration of 0.2% (v/v). Percent release was calculated as $((F–F_0)/(F_{100}–F_0)) \times 100$, where F is the observed fluorescence at a given time, and F_0 and F_{100} represent baseline and maximal fluorescence, respectively.

Competition STD NMR—Individual fragments were added to 5 μM BAX with or without 5 μM competitor peptide in 20 mM potassium phosphate buffer, pH 6.2. STD NMR was measured as described above. Fragments that were competed by peptide showed a decreased saturation transfer difference in the presence of peptide relative to no peptide.

CPMG NMR—CPMG experiments were performed using standard methods[53]. NMR analyses employed BIF-44 at a concentration of 300 μM, with or without added BAX (5 μM), in a 20 mM potassium phosphate buffer, pH 6.2. A 0.5 millisecond tau delay (1 ms per CPMG echo cycle) was applied, with the number of echo cycles corresponding to 500 ms. Excitation sculpting was used for solvent suppression, as reported[54].

NMR-based detection of small molecule aggregators—To detect line broadening, standard ^{1}H-NMR spectra were acquired. T2 decay curves were generated by measuring the CPMG NMR spectra of the molecules, performed as described above. The number of echo cycles corresponds to the decay time. The intensity of the aromatic peaks at the indicated decay times were measured and normalized to a maximum intensity of 1 at the 10 ms decay time. The curves were fitted to a one phase decay model using Prism software (Graphpad). Excitation sculpting was used for solvent suppression. Samples for both analyses were prepared in 20 mM potassium phosphate buffer, pH 6.2, 10% (v/v) D_2O.

Dynamic light scattering—The indicated molecules were diluted from a 100 mM stock into 20 mM potassium phosphate buffer, pH 6.2, with a final DMSO concentration of 1%. Samples were analyzed at room temperature on a DynaPro-99 instrument equipped with a 90° detector angle using a 10 second acquisition time per measurement.

Negative stain electron microscopy—Small molecules were diluted from 100 mM DMSO stocks in 20 mM Tris-HCl, pH 7.2 to 100 μM for I4PTH, and 300 μM for 4-ADPA and BIF-44. Samples were then applied to a glow discharged carbon-coated grid (Electron Microscopy Sciences) for 60 seconds. The grid was blotted on filter paper to remove excess solution, washed once in water, and stained with 1% (w/v) uranyl formate for 20 seconds. Images were acquired using a JEOL JEM1200 EX transmission electron microscope (Harvard Medical School Electron Microscopy Facility).

Isothermal titration calorimetry—Binding affinity was measured by adding 0.15 mM recombinant BAX protein to the cell and injecting 2.0 μL of 1.0 mM ligand by syringe for a total of 30 injections using an Affinity ITC (TA instruments) at 25°C. BAX and BIF-44 solutions were prepared in 20 mM potassium phosphate buffer (pH 6.2), with a final concentration of 2% (v/v) DMSO. The samples were centrifuged for 15 min at 4°C before

titration. ITC experiments were performed in duplicate and the data analyzed with the NanoAnalyze software package (TA instruments) using a single binding site model and thermodynamic parameters calculated as follows: $\Delta G = \Delta H - T\Delta S = -RT\ln K_{B,}$ where ΔG, ΔH and ΔS are the changes in free energy, enthalpy and entropy of binding, respectively.

Fluorescence polarization assay

FITC-peptide (25 nM) was incubated with a serial dilution of recombinant, full-length BAX in binding buffer (20 mM potassium phosphate, pH 6.2). For competitive FP, FITC-peptide (25 nM) was mixed with a fixed concentration of BAX (250 nM) and incubated with a serial dilution of acetylated peptide or molecular fragment. Fluorescence polarization was measured at equilibrium using a SpectraMax M5 microplate reader. Nonlinear regression analysis of dose-response curves was performed using Prism software 7 (GraphPad).

HSQC NMR—Uniformly ^{15}N-labeled recombinant BAX (50 μM) was generated as previously described[1,6]. Protein samples with the indicated molar ratio of fragment were prepared in 25 mM sodium phosphate, 50 mM NaCl solution at pH 6.0 in 10% (v/v) D_2O. Correlation ^{1}H-^{15}N HSQC spectra were acquired at 25°C on a Bruker 600 MHz NMR spectrometer equipped with a cryogenic probe, processed in Topspin (Bruker) and analyzed using CcpNmr Analysis[55]. The weighted average chemical shift difference was calculated as $\Delta = \sqrt{1/2 \times ((\Delta \mathrm{H})^2 + (\Delta N/5)^2)}$[56], where ΔH and ΔN are the respective changes in p.p.m. of ^{1}H or ^{15}N for the indicated crosspeak. The absence of a bar indicates no chemical shift difference, or the presence of a proline or residue that is overlapped or not assigned. BAX cross-peak assignments were applied as previously reported[1]. The significance threshold for the chemical shift changes was calculated based on the average chemical shift across all residues plus the standard deviation, in accordance with standard methods[5,6].

Molecular docking—The Schrödinger software suite (Version 2016-2) was used for docking calculations. Conformations of molecule BIF-44 were generated in MacroModel using the OPLS3 forcefield. Each of the 20 NMR conformations of BAX (PDB ID 1F16) was separately prepared using the default parameters in the PrepWiz wizard in Maestro. The docking receptor grid (radius 1 nm) was defined at the center of Ala124, the amino acid with the greatest HSQC shift. BIF-44 was then docked onto all 20 structures using Glide Extra Precision (XP) mode. The top-scoring poses were then manually inspected for consistency with experimentally-determined HSQC shifts for the complex. The FTsite (https://ftsite.bu.edu/) and FTdyn (https://ftdyn.bu.edu/) web servers were used for binding site prediction and dynamic ensemble mapping, respectively[40]. All site prediction analyses were run using default parameters.

Molecular dynamics simulation—Starting structures for MD calculations included the first NMR structure of BAX from PDB ID 1F16 and the BIF-44/BAX complex generated by molecular docking. The protein was prepared using the default parameters of the Protein Preparation Workflow in Maestro software (Schrödinger Version 2016-2). Protonation states were those predicted to occur at pH 7.0 using the Epik module. Protein was pre-soaked in a cubic box of TIP3P water molecules using the System Builder workflow in Desmond. The box was sized such that all peptide atoms were at least 1 nm from the boundaries. All

overlapping solvent molecules were removed, the system was charge neutralized with appropriate counterions, and 150 mM NaCl was added to simulate buffer conditions. All MD simulations were performed using the Desmond package, with the OPLS3 forcefield applied to model all interactions. Periodic boundary conditions were maintained throughout. Long-range electrostatic interactions were calculated using the particle-mesh Ewald method, and van der Waals and short-range electrostatic interactions were smoothly truncated at 0.9 nm. Constant system temperature of 300 K was maintained using Nose-Hoover thermostats, and system pressure was maintained at 1 atm using the Martina-Tobias-Klein method. The equations of motion were integrated using the RESPA integrator, with a 2.0 fs timestep for bonded and short-range interactions and a 6.0 fs timestep for non-bonded interactions beyond the 0.9 nm cutoff. The default parameters in Desmond were used to relax the system prior to simulation. Following this procedure, a 100 ns production simulation was run and configurations saved at 4 ps intervals. All simulations were judged to have converged on the basis of radius of gyration calculations and RMSD. Principal component analysis was conducted using the Bio3D package[57,58]. All-atom elastic network model normal mode analysis (aaNMA) was performed using the Bio3D package[57,59] and the aaenm2 forcefield. The first three non-trivial normal modes were analyzed as both trajectories and per-residue fluctuations.

Hydrogen-deuterium exchange mass spectrometry—Hydrogen-deuterium exchange mass spectrometry (HXMS) experiments were performed as described[7,48]. Deuterium labeling was initiated with an 18-fold dilution into D_2O buffer (10 mM HEPES, 200 mM KCl, 1 mM $MgCl_2$, pD 6.6) of a pre-equilibrated (15 min, room temperature) aliquot of each BAX protein (30 μM), molecule, peptide, and/or antibody (BAX BH3, Abgent AP1302a; BAX 6A7, Santa Cruz Biotechnology sc-23959) mixture. At the indicated time points, the labeling reaction was quenched with the addition of an equal volume of quench buffer (0.8 M guanidinium chloride, 0.8% formic acid [v/v]). Each deuterium labeling experiment was performed in at least duplicate. Proteolysis was performed by incubation on ice with 40 μg pepsin and 20 μg factor XIII (both at 10 mg/mL in water) for 5 min. Digested samples were then processed and analyzed as described previously[7]. Briefly, the peptides were trapped and desalted on a VanGuard Pre-Column trap (2.1 × 5 mm, ACQUITY UPLC BEH C18, 1.7 μm) for 3 min, eluted from the trap using a 5–35% gradient of acetonitrile over 6 min at a flow rate of 65 μL/min, and then separated using an ACQUITY UPLC HSS T3, 1.8 μm, 1.0 × 50 mm column. Peptides from an unlabeled protein were identified using ProteinLynx Global Server (PLGS) searches of a protein database including analyte protein. All mass spectra were acquired using a Waters SYNAPT G2 or G2Si mass spectrometer. The relative deuterium levels of identified peptides common to all evaluated conditions are shown. The error of determining the average deuterium incorporation for each peptide was at or below ± 0.25 Da. Relative deuterium levels for each peptide were calculated by subtracting the average mass of the undeuterated control sample from that of the deuterium-labeled sample. All mass spectra were processed using DynamX 3.0 (Waters Corporation). Deuterium levels were not corrected for back exchange and thus reported as relative.

Mitochondrial cytochrome *c* release assay—Liver mitochondria from $Alb^{Cre}Bax^{f/f}Bak^{-/-}$ mice were isolated and release assays performed as described[52]. Briefly, mitochondria (0.5 mg/mL) were incubated with 100 nM BAX, 250 nM BIM $SAHB_{A2}$ and/or the indicated concentrations of BIF-44 for 45 min at room temperature in experimental buffer (200 mM mannitol, 68 mM sucrose, 10 mM HEPES-KOH [pH 7.4], 110 mM KCl, 1 mM EDTA, protease inhibitor)[60]. The pellet and supernatant fractions were isolated by centrifugation, and cytochrome *c* was quantitated using a colorimetric ELISA assay (R&D Systems), per the manufacturer's protocol. Percent cytochrome *c* released into the supernatant (%cyto *c* release) was calculated according to the following equation: %cyto *c* release = [cyto c_{sup}]/[cyto c_{max}]*100, where cyto c_{sup} and cyto c_{max} represent the amount of cytochrome *c* detected in the supernatant of compound- or 1% (v/v) Triton X-100-treated samples, respectively. Animal experiments involving the harvest of mouse liver mitochondria for cytochrome *c* release assays were approved by and performed in accordance with the guidelines and regulations set forth by the Institutional Animal Care and Use Committee of the Dana-Farber Cancer Institute.

Statistical methods—Statistical significance was calculated by one-way ANOVA analysis using Prism software (Graphpad). *P* values of less than 0.05 were considered significant.

Data Availability

The data generated and analyzed for this study are included in the published article and its supplementary information files. Any additional requests can be directed to the corresponding author.

Supplementary Material

Refer to Web version on PubMed Central for supplementary material.

Acknowledgments

We thank E. Smith for graphics support, C. Sheahan for operational assistance with the NMR screen, M. Godes for assistance with mitochondrial preparation, G. Bird and T. Oo for peptide production, M. Ericsson and Z. Hauseman for technical assistance with electron microscopy, H.-S. Seo and S. Dhe-Paganon for ITC experiments, and D. Andrews and K. Sarosiek for providing BIM_L plasmid and protein, respectively. This research was supported by NIH grant 1R35CA197583, a Leukemia and Lymphoma Society (LLS) Scholar Award, the Todd J. Schwartz Memorial Fund, the Wolpoff Family Foundation, and a grant from the William Lawrence and Blanche Hughes Foundation to L.D.W.; NIH grant R01GM101135 to J.R.E. and a research collaboration with the Waters Corporation (J.R.E.); NIH grant F31CA189651 to J.R.P.; an Alexander von Humboldt Foundation Feodor Lynen Fellowship to F.W.; and NIH training grant T32GM007753 to J.L.

References

1. Suzuki M, Youle RJ, Tjandra N. Structure of Bax: coregulation of dimer formation and intracellular localization. Cell. 2000; 103:645–54. [PubMed: 11106734]
2. Edlich F, et al. Bcl-x(L) retrotranslocates Bax from the mitochondria into the cytosol. Cell. 2011; 145:104–16. [PubMed: 21458670]
3. Czabotar PE, et al. Bax crystal structures reveal how BH3 domains activate Bax and nucleate its oligomerization to induce apoptosis. Cell. 2013; 152:519–31. [PubMed: 23374347]

4. Edwards AL, et al. Multimodal interaction with BCL-2 family proteins underlies the proapoptotic activity of PUMA BH3. Chem Biol. 2013; 20:888–902. [PubMed: 23890007]
5. Gavathiotis E, Reyna DE, Davis ML, Bird GH, Walensky LD. BH3-triggered structural reorganization drives the activation of proapoptotic BAX. Mol Cell. 2010; 40:481–92. [PubMed: 21070973]
6. Gavathiotis E, et al. BAX activation is initiated at a novel interaction site. Nature. 2008; 455:1076–81. [PubMed: 18948948]
7. Barclay LA, et al. Inhibition of Pro-apoptotic BAX by a noncanonical interaction mechanism. Mol Cell. 2015; 57:873–86. [PubMed: 25684204]
8. Ma J, et al. Structural mechanism of Bax inhibition by cytomegalovirus protein vMIA. Proc Natl Acad Sci U S A. 2012; 109:20901–6. [PubMed: 23213219]
9. Petros AM, et al. Solution structure of the antiapoptotic protein bcl-2. Proc Natl Acad Sci U S A. 2001; 98:3012–7. [PubMed: 11248023]
10. Walensky LD, Gavathiotis E. BAX unleashed: the biochemical transformation of an inactive cytosolic monomer into a toxic mitochondrial pore. Trends Biochem Sci. 2011; 36:642–52. [PubMed: 21978892]
11. Souers AJ, et al. ABT-199, a potent and selective BCL-2 inhibitor, achieves antitumor activity while sparing platelets. Nat Med. 2013; 19:202–8. [PubMed: 23291630]
12. Sattler M, et al. Structure of Bcl-xL-Bak peptide complex: recognition between regulators of apoptosis. Science. 1997; 275:983–6. [PubMed: 9020082]
13. Lessene G, et al. Structure-guided design of a selective BCL-X(L) inhibitor. Nat Chem Biol. 2013; 9:390–7. [PubMed: 23603658]
14. Tao ZF, et al. Discovery of a Potent and Selective BCL-XL Inhibitor with in Vivo Activity. ACS Med Chem Lett. 2014; 5:1088–93. [PubMed: 25313317]
15. Tse C, et al. ABT-263: a potent and orally bioavailable Bcl-2 family inhibitor. Cancer Res. 2008; 68:3421–8. [PubMed: 18451170]
16. Bruncko M, et al. Structure-guided design of a series of MCL-1 inhibitors with high affinity and selectivity. J Med Chem. 2015; 58:2180–94. [PubMed: 25679114]
17. Cohen NA, et al. A competitive stapled peptide screen identifies a selective small molecule that overcomes MCL-1-dependent leukemia cell survival. Chem Biol. 2012; 19:1175–86. [PubMed: 22999885]
18. Kotschy A, et al. The MCL1 inhibitor S63845 is tolerable and effective in diverse cancer models. Nature. 2016; 538:477–482. [PubMed: 27760111]
19. Leverson JD, et al. Potent and selective small-molecule MCL-1 inhibitors demonstrate on-target cancer cell killing activity as single agents and in combination with ABT-263 (navitoclax). Cell Death Dis. 2015; 6:e1590. [PubMed: 25590800]
20. Pelz NF, et al. Discovery of 2-Indole-acylsulfonamide Myeloid Cell Leukemia 1 (Mcl-1) Inhibitors Using Fragment-Based Methods. J Med Chem. 2016; 59:2054–66. [PubMed: 26878343]
21. Stewart ML, Fire E, Keating AE, Walensky LD. The MCL-1 BH3 helix is an exclusive MCL-1 inhibitor and apoptosis sensitizer. Nat Chem Biol. 2010; 6:595–601. [PubMed: 20562877]
22. Huhn AJ, Guerra RM, Harvey EP, Bird GH, Walensky LD. Selective Covalent Targeting of Anti-Apoptotic BFL-1 by Cysteine-Reactive Stapled Peptide Inhibitors. Cell Chem Biol. 2016; 23:1123–34. [PubMed: 27617850]
23. Gavathiotis E, Reyna DE, Bellairs JA, Leshchiner ES, Walensky LD. Direct and selective small-molecule activation of proapoptotic BAX. Nat Chem Biol. 2012; 8:639–45. [PubMed: 22634637]
24. Brahmbhatt H, Uehling D, Al-Awar R, Leber B, Andrews D. Small molecules reveal an alternative mechanism of Bax activation. Biochem J. 2016; 473:1073–83. [PubMed: 26916338]
25. Xin M, et al. Small-molecule Bax agonists for cancer therapy. Nat Commun. 2014; 5:4935. [PubMed: 25230299]
26. Zhao G, et al. Activation of the proapoptotic Bcl-2 protein Bax by a small molecule induces tumor cell apoptosis. Mol Cell Biol. 2014; 34:1198–207. [PubMed: 24421393]
27. Wang K, Gross A, Waksman G, Korsmeyer SJ. Mutagenesis of the BH3 domain of BAX identifies residues critical for dimerization and killing. Mol Cell Biol. 1998; 18:6083–9. [PubMed: 9742125]

28. Scott DE, Coyne AG, Hudson SA, Abell C. Fragment-based approaches in drug discovery and chemical biology. Biochemistry. 2012; 51:4990–5003. [PubMed: 22697260]
29. Mayer M, Meyer B. Characterization of Ligand Binding by Saturation Transfer Difference NMR Spectroscopy. Angewandte Chemie International Edition. 1999; 38:1784–1788.
30. Stockman BJ, Dalvit C. NMR screening techniques in drug discovery and drug design. Progress in Nuclear Magnetic Resonance Spectroscopy. 2002; 41:187–231.
31. Tan C, et al. Auto-activation of the apoptosis protein Bax increases mitochondrial membrane permeability and is inhibited by Bcl-2. J Biol Chem. 2006; 281:14764–75. [PubMed: 16571718]
32. Wei MC, et al. tBID, a membrane-targeted death ligand, oligomerizes BAK to release cytochrome c. Genes Dev. 2000; 14:2060–71. [PubMed: 10950869]
33. Pagliari LJ, et al. The multidomain proapoptotic molecules Bax and Bak are directly activated by heat. Proc Natl Acad Sci U S A. 2005; 102:17975–80. [PubMed: 16330765]
34. Sarosiek KA, et al. BID preferentially activates BAK while BIM preferentially activates BAX, affecting chemotherapy response. Mol Cell. 2013; 51:751–65. [PubMed: 24074954]
35. McGovern SL, Helfand BT, Feng B, Shoichet BK. A specific mechanism of nonspecific inhibition. J Med Chem. 2003; 46:4265–72. [PubMed: 13678405]
36. Irwin JJ, et al. An Aggregation Advisor for Ligand Discovery. J Med Chem. 2015; 58:7076–87. [PubMed: 26295373]
37. Julien O, et al. Unraveling the mechanism of cell death induced by chemical fibrils. Nat Chem Biol. 2014; 10:969–76. [PubMed: 25262416]
38. Arnoult D, et al. Cytomegalovirus cell death suppressor vMIA blocks Bax- but not Bak-mediated apoptosis by binding and sequestering Bax at mitochondria. Proc Natl Acad Sci U S A. 2004; 101:7988–93. [PubMed: 15148411]
39. Poncet D, et al. An anti-apoptotic viral protein that recruits Bax to mitochondria. J Biol Chem. 2004; 279:22605–14. [PubMed: 15004026]
40. Kozakov D, et al. The FTMap family of web servers for determining and characterizing ligand-binding hot spots of proteins. Nat Protoc. 2015; 10:733–55. [PubMed: 25855957]
41. Engen JR. Analysis of protein conformation and dynamics by hydrogen/deuterium exchange MS. Anal Chem. 2009; 81:7870–5. [PubMed: 19788312]
42. Laiken SL, Printz MP, Craig LC. Tritium-hydrogen exchange studies of protein models. I. Gramicidin S-A. Biochemistry. 1969; 8:519–26. [PubMed: 5793708]
43. Printz MP, Williams HP, Craig LC. Evidence for the presence of hydrogen-bonded secondary structure in angiotensin II in aqueous solution. Proc Natl Acad Sci U S A. 1972; 69:378–82. [PubMed: 4333981]
44. Shi XE, et al. Hydrogen exchange-mass spectrometry measures stapled peptide conformational dynamics and predicts pharmacokinetic properties. Anal Chem. 2013; 85:11185–8. [PubMed: 24215480]
45. Hsu YT, Youle RJ. Nonionic detergents induce dimerization among members of the Bcl-2 family. J Biol Chem. 1997; 272:13829–34. [PubMed: 9153240]
46. Goping IS, et al. Regulated targeting of BAX to mitochondria. J Cell Biol. 1998; 143:207–15. [PubMed: 9763432]
47. Follis AV, et al. PUMA binding induces partial unfolding within BCL-xL to disrupt p53 binding and promote apoptosis. Nat Chem Biol. 2013; 9:163–8. [PubMed: 23340338]
48. Lee S, et al. Allosteric inhibition of antiapoptotic MCL-1. Nat Struct Mol Biol. 2016; 23:600–7. [PubMed: 27159560]
49. Oltersdorf T, et al. An inhibitor of Bcl-2 family proteins induces regression of solid tumours. Nature. 2005; 435:677–81. [PubMed: 15902208]
50. Leshchiner ES, Braun CR, Bird GH, Walensky LD. Direct activation of full-length proapoptotic BAK. Proc Natl Acad Sci U S A. 2013; 110:E986–95. [PubMed: 23404709]
51. Bird GH, Crannell WC, Walensky LD. Chemical synthesis of hydrocarbon-stapled peptides for protein interaction research and therapeutic targeting. Curr Protoc Chem Biol. 2011; 3:99–117. [PubMed: 23801563]

52. Pitter K, Bernal F, Labelle J, Walensky LD. Dissection of the BCL-2 family signaling network with stabilized alpha-helices of BCL-2 domains. Methods Enzymol. 2008; 446:387–408. [PubMed: 18603135]

53. Hajduk PJ, Olejniczak ET, Fesik SW. One-Dimensional Relaxation- and Diffusion-Edited NMR Methods for Screening Compounds That Bind to Macromolecules. J Am Chem Soc. 1997; 119:12257–12261.

54. Hwang T, Shaka AJ. Water Suppression That Works. Excitation Sculpting Using Arbitrary Waveforms and Pulsed Field Gradients. J Magn Reson A. 1995; 112:275–279.

55. Vranken WF, et al. The CCPN data model for NMR spectroscopy: development of a software pipeline. Proteins. 2005; 59:687–96. [PubMed: 15815974]

56. Williamson MP. Using chemical shift perturbation to characterise ligand binding. Prog Nucl Magn Reson Spectrosc. 2013; 73:1–16. [PubMed: 23962882]

57. Grant BJ, Rodrigues AP, ElSawy KM, McCammon JA, Caves LS. Bio3d: an R package for the comparative analysis of protein structures. Bioinformatics. 2006; 22:2695–6. [PubMed: 16940322]

58. Skjaerven L, Yao XQ, Scarabelli G, Grant BJ. Integrating protein structural dynamics and evolutionary analysis with Bio3D. BMC Bioinformatics. 2014; 15:399. [PubMed: 25491031]

59. Yao XQ, Skjaerven L, Grant BJ. Rapid Characterization of Allosteric Networks with Ensemble Normal Mode Analysis. J Phys Chem B. 2016; 120:8276–88. [PubMed: 27056373]

60. Llambi F, et al. A unified model of mammalian BCL-2 protein family interactions at the mitochondria. Mol Cell. 2011; 44:517–31. [PubMed: 22036586]

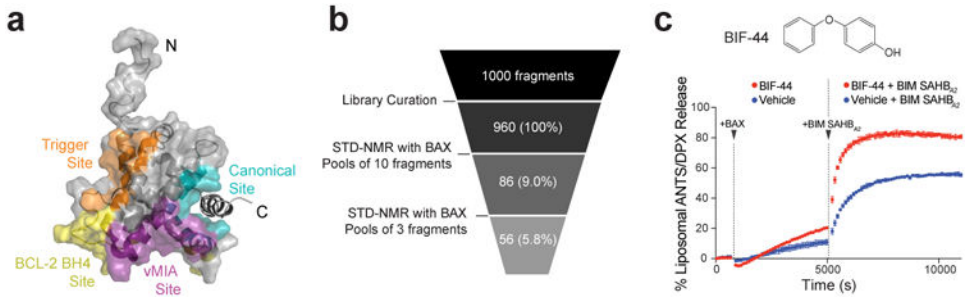

Figure 1. STD NMR-based identification of BAX-interacting fragments that modulate BH3-mediated BAX activation

(**a**) BAX contains a series of surface grooves that regulate its pro-apoptotic activity, including the activating BH3 trigger (orange) and canonical (cyan) sites, and inhibitory BCL-2 BH4 (yellow) and vMIA (purple) interaction pockets. (**b**) Identification of BAX-interacting fragments (BIFs) by sequential STD NMR screening in pools of 10, 3, and then singlet, yielding 56 candidate BIFs. BAX, 5 μM; Molecules, 300 μM (**c**) BIF-44 has no independent effect on the liposomes (red, left), minimal direct BAX activation activity (red, middle), but notably enhances the kinetics and quantity of liposomal release upon addition of BIM SAHB$_{A2}$ (red, right), exceeding the maximal level of release achieved by the BIM SAHB$_{A2}$ and BAX combination alone (blue, right). Error bars are mean ± SD for experiments performed in technical triplicate, and repeated twice more with similar results using independent liposomal and protein preparations. BAX, 0.75 μM; BIM SAHB$_{A2}$, 0.75 μM; BIF-44, 113 μM (150×)

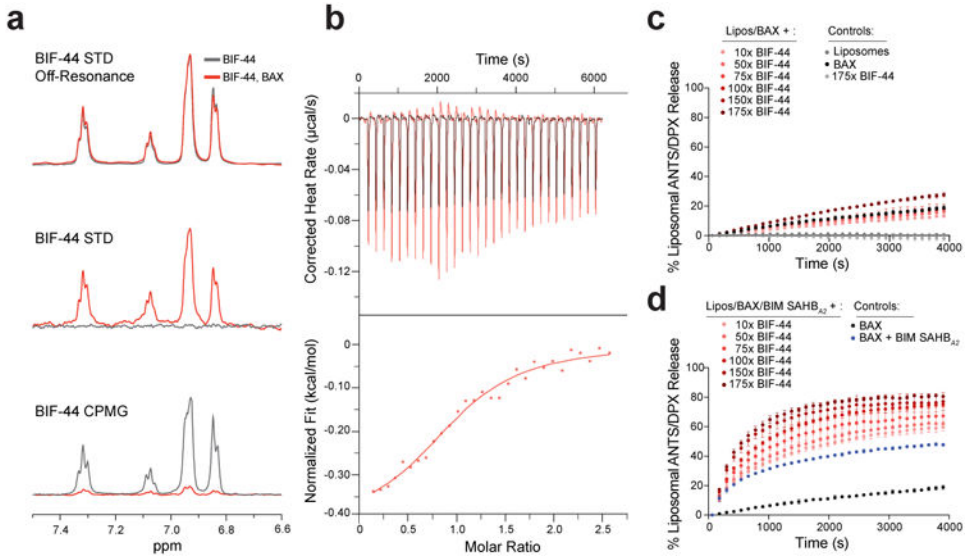

Figure 2. Validation of BIF-44 as a dose-responsive binder and sensitizer of BAX

(**a**) NMR analyses of BIF-44 in the presence (red) and absence (gray) of BAX protein: STD off resonance (top), STD (middle), CPMG (500 ms) (bottom). BAX, 5 μM; BIF-44, 300 μM (**b**) Isothermal titration calorimetry analysis of the BIF-44/BAX interaction. ITC was performed in duplicate with a representative analysis shown (single binding site model; BAX, 150 μM; K_d, 37 ± 12 μM). (**c**, **d**) Liposomal release assays demonstrate little to no direct, BAX-activating effect of BIF-44 across a broad dose range (**c**), but dose-responsively sensitizes BH3-triggered direct BAX activation upon co-incubation with BIM SAHB$_{A2}$ (**d**). Error bars are mean ± SD for experiments performed in technical triplicate and repeated twice more with similar results using independent liposomal and protein preparations. BAX, 0.75 μM; BIM SAHB$_{A2}$ 0.75 μM; BIF-44, 7.5 μM–131 μM (10×–175×)

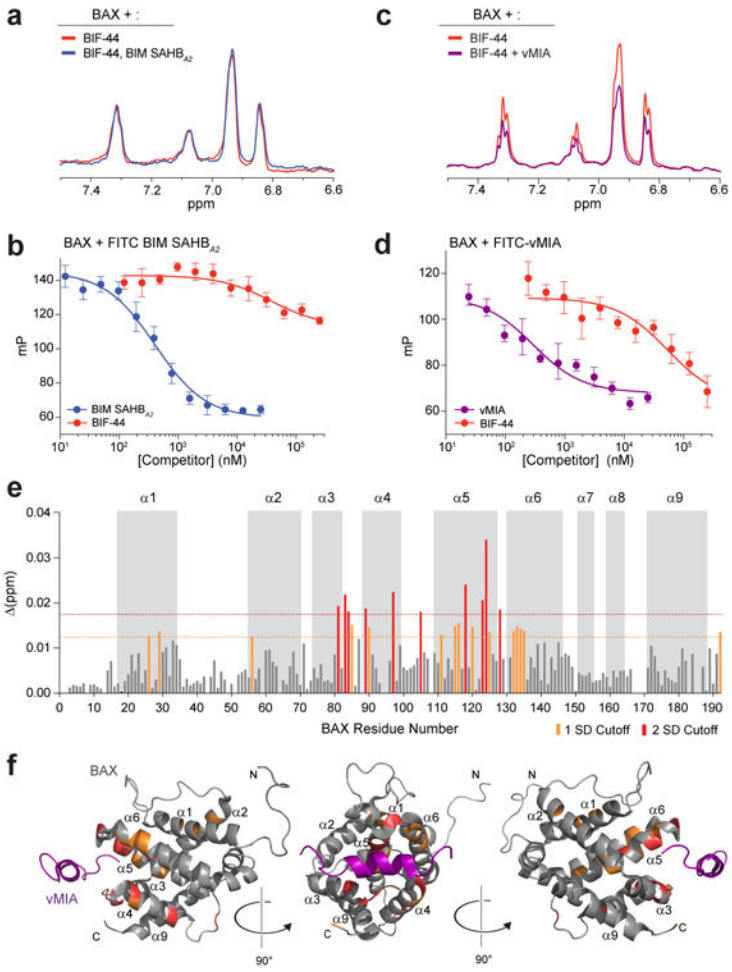

Figure 3. BIF-44 targets the vMIA-binding region of BAX

(**a–d**) Competitive STD NMR and fluorescence polarization (FP) analyses of the BIF-44/BAX interaction in the presence of BIM SAHB$_{A2}$ (**a,b**) or vMIA peptide (**c,d**). NMR data are representative of two independent experiments; BAX, 5 μM; BIM SAHB$_{A2}$ or vMIA peptide 5 μM; BIF-44, 300 μM. For FP, error bars are mean ± SD for experiments performed in technical quadruplicate and repeated with similar results using independent reagent preparations. FITC-peptides, 25 nM; BAX, 250 nM. (**e**) Measured chemical shift changes of ^{15}N-BAX (50 μM) upon addition of BIF-44 (6:1, BIF:BAX), plotted as a function of BAX residue number. Chemical shift changes above the 2 SD cutoff (≥ 0.018 ppm significance threshold) are colored red and localize to the junction of the α3/α4 and α5/α6 hairpins. Significant changes at the 1 SD cutoff (≥ 0.012 ppm significance threshold) are colored orange and encompass internal residues of the α5 and α6 core and discrete, juxtaposed residues of α1 and α2. (**f**) Residues represented as red and orange bars in (**e**) are mapped onto the ribbon diagrams of BAX (PDB ID 2LR1). The most prominent chemical shift changes (2 SD cutoff) localize to the region implicated in the vMIA (purple) interaction. A second cluster of chemical shift changes (1 SD cutoff) localize to internal and juxtaposed residues of α5, α6 and α1, α2, suggestive of allosteric sensing from the adjacent hydrophobic core to the α1–loop–α2 region of the BAX N-terminal face.

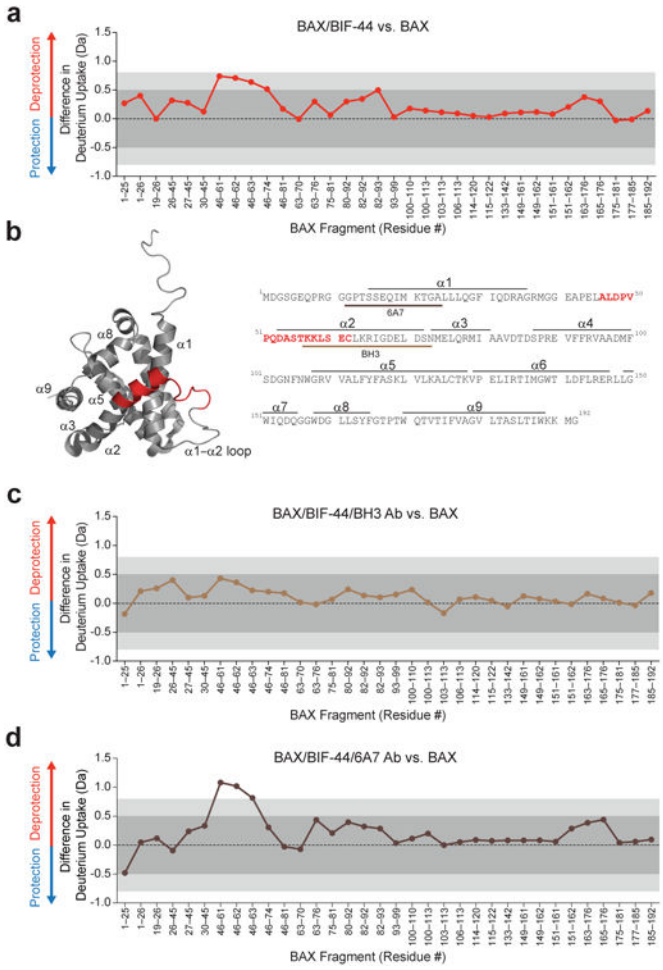

Figure 4. Allosteric deprotection of the α1–α2 loop and BAX BH3 domain upon BIF-44 binding

(**a**,**b**) The addition of BIF-44 to BAX (30 μM, 10:1 BIF:BAX, 15 min incubation/10 sec deuteration) in a liposomal environment triggered a regiospecific increase in deuterium incorporation compared to unliganded BAX, as measured by HXMS (**a**). The difference in deuterium uptake plot reflects the relative deuterium incorporation of BIF-44/BAX minus the relative deuterium incorporation of BAX. Dark gray shading, changes below significance threshold of 0.5 Da; light gray shading and white region, changes above significance thresholds of 0.5 Da and 0.8 Da, respectively. Data are representative of two independent experiments. (**b**) The region of BIF-44-induced deprotection encompasses peptide fragments corresponding to amino acids 46–62, which are highlighted in red on the ribbon diagram (left, PDB ID 1F16) and amino acid sequence (right), and map to the critical α1–α2 loop and BH3 regions of BAX. (**c, d**) The deprotection induced by BIF-44 is suppressed by co-incubation with an anti-BAX BH3 antibody (30 μM BAX, 1:10:0.5 BAX:BIF-44:antibody) (**c**), but not the BAX 6A7 antibody (**d**), which binds to N-terminal residues of conformationally-activated BAX. The BAX amino acid sequences recognized by the BAX BH3 and 6A7 antibodies are underlined in tan and brown, respectively (**b**). The difference in deuterium uptake plots reflect the relative deuterium incorporation of BIF-44/BAX/BH3 Ab

(**c**) and BIF-44/BAX/6A7 Ab (**d**) minus the relative deuterium incorporation of BAX, as measured at 10 sec. Data are representative of two independent experiments.

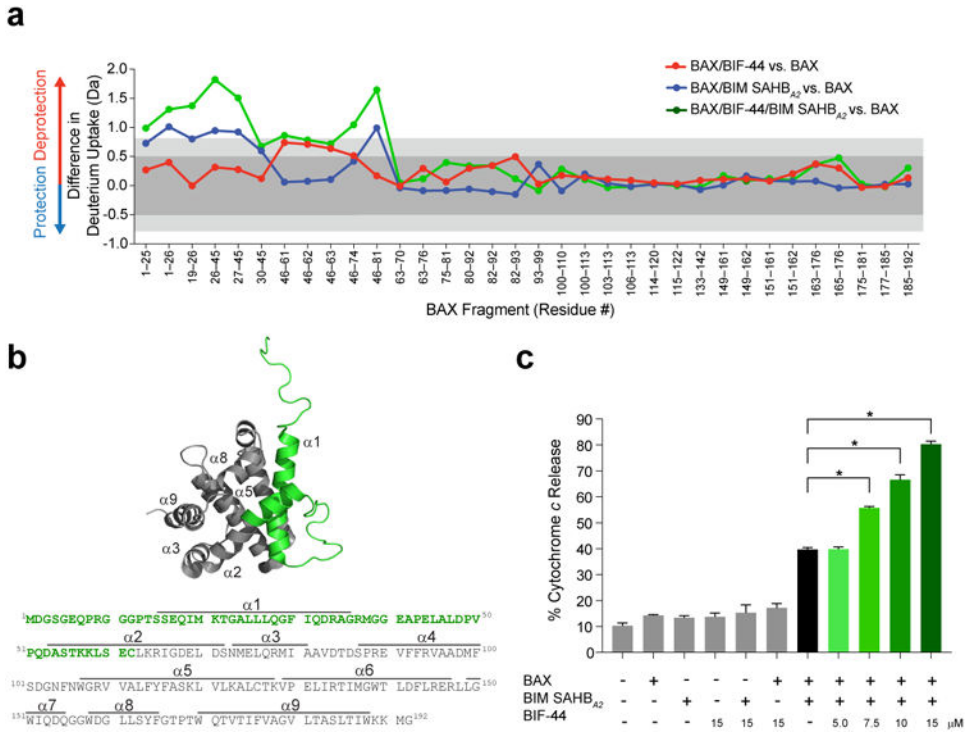

Figure 5. BIF-44 sensitizes the BH3-triggered conformational activation and cytochrome *c* release activity of BAX

(**a**) Comparative HXMS profiles of BAX in the presence of liposomes upon exposure to BIF-44 (red), BIM SAHB$_{A2}$ (blue), or both ligands (green). The difference in deuterium uptake plots reflect the relative deuterium incorporation of BIF-44/BAX (red), BIM SAHB$_{A2}$/BAX (blue), and BIF-44/BIM SAHB$_{A2}$/BAX (green) minus the relative deuterium incorporation of BAX, as measured at 10 sec (BAX 30 μM, 10× BIF-44, 1× peptide). Dark gray shading represents changes in the plot that are below the significance threshold of 0.5 Da, whereas light gray shading and the white region highlight changes above the baseline significance threshold of 0.5 Da and the more stringent threshold of 0.8 Da, respectively. Data are representative of two independent experiments. (**b**) The prominent region of deprotection (α1, α1–α2 loop, and α2) induced by treating BAX with the synergistic BIF-44/BIM SAHB$_{A2}$ combination is highlighted in green on the ribbon diagram (PDB ID: 1F16) and amino acid sequence. (**c**) BIF-44 dose-responsively sensitizes BIM SAHB$_{A2}$-triggered, BAX-mediated cytochrome *c* release from isolated *Alb*^{Cre}*Bax*$^{f/f}$*Bak*$^{-/-}$ mouse liver mitochondria. Error bars are mean ± SD for experiments performed in technical triplicate, and repeated twice more with similar results using independent preparations and treatments of mitochondria. 100 nM BAX, 250 nM BIM SAHB$_{A2}$, BIF-44, 5–15 μM; *, $p < 0.001$, as calculated by one-way ANOVA analysis.